Gondwana Research 64 (2018) 1–10

Contents lists available at ScienceDirect

Gondwana Research

journal homepage: www.elsevier.com/locate/gr

Post-collisional exhumation of the Indus-Yarlung suture zone and Northern Tethyan Himalaya, Saga, SW Tibet

Guangwei Li [a,*], Barry Kohn [a], Mike Sandiford [a], Zeliang Ma [b], Zhiqin Xu [b]

[a] School of Earth Sciences, University of Melbourne, Melbourne 3010, Australia
[b] The Department of Earth Sciences, Nanjing University, Nanjing, China

ARTICLE INFO

Article history:
Received 13 February 2018
Received in revised form 31 May 2018
Accepted 18 June 2018
Available online 16 August 2018

Handling Editor: Z.M. Zhang

Keywords:
Sangdanlin
Tethyan Himalaya
Low temperature thermochronology
Yarlung River
South Tibet

ABSTRACT

The Cretaceous-Eocene sedimentary sequences of the Sangdanlin section at Saga, SW Tibet, within the India-Asia collisional zone, have been studied in detail for constraining the timing of initial collision. However, the post-depositional history has not been investigated. Here, we report new low temperature thermochronology data along the classic Sangdanlin section, to reveal the cooling/exhumation history of the Indus-Yarlung suture zone (IYSZ) and northern Tethyan Himalaya. Samples from the IYSZ, all yield latest Oligocene-Miocene ages, with most zircon (U-Th)/He ages ranging between ~18 and 27 Ma and apatite fission track (AFT) ages of ~12–9 Ma. Thermal history modelling indicates a consistent Middle-Late Miocene cooling episode related to post-Great Counter Thrust (GCT) incision of the Yarlung River. To the south, samples from the northern Tethyan Himalaya Mesozoic sequences yield older ZHe ages of ~32–36 Ma, signifying activity of the Tethyan Himalayan fold-thrust zone, while two granites linked to formation of the North Himalayan gneiss domes yield Late Miocene AFT ages. The regional low temperature thermochronology data reveal different cooling patterns for tributaries on the northern and southern sides of the Yarlung River. This points to the strong influence of Early Miocene tectonism along the GCT, as a major controlling factor on river drainage reorganization at this time.

1. Introduction

In the two decades, low temperature thermochronology (e.g. apatite fission track-AFT, zircon/apatite U-Th/He - ZHe/AHe), has emerged as a powerful tool for revealing the timing of cooling and exhumation histories of orogenic belts (e.g. Reiners, 2005; Thiede and Ehlers, 2013). In the Himalayan orogen, many low temperature thermochronology studies have focused on crystalline basement rocks, such as the Gangdese batholith (e.g. Dai et al., 2013; Li et al., 2016; Ge et al., 2017; Rohrmann et al., 2012; references therein), and the Greater Himalayas (e.g. Thiede and Ehlers, 2013; Wilke et al., 2012; references therein). Although some recent low temperature thermochronology data have been reported from sedimentary sequences within the orogen (e.g. Carrapa et al., 2014; Li et al., 2015a,c; G.-W. Li et al., 2017; Orme, 2017; Shen et al., 2016), there are still large data gaps within sedimentary matrix mélanges within the Indus-Yarlung suture zone and Tethyan Himalaya, especially in the central and west Himalaya. Further, several AFT studies conducted in the region focused on apparent thermochronology ages, without length measurements because of experimental limitations. If such data is incorporated into thermal history modelling, it will only provide simplistic solutions and cannot reveal any complexities in the timing of the cooling events. Hence, details of the post-collisional exhumation of the Himalaya in South Tibet remains less well constrained.

In this work, we investigate the sedimentary sequences of the Sangdanlin section in Saga, southwest Tibet, which have been well documented for revealing initial India-Asia collision processes (e.g. DeCelles et al., 2014; Hu et al., 2015; Wu et al., 2014), as well as adjacent northern Tethyan Himalaya. Using thermal history modelling of low temperature thermochronology (AFT and ZHe) data, we further constrain the regional post-collisional cooling history, and late Cenozoic deformation. Furthermore, the study area, is located within the catchment of the Yarlung River, forming one of the major drainage systems in the Himalaya and has been eroded by river incision. In combination with previous low temperature thermochronology dataset, this work will also discuss the incision history for tributaries of the Yarlung River, to shed light on the regional cooling/exhumation history in the Himalayan orogeny.

2. Geological setting

The Indus-Yarlung suture zone (IYSZ) marks the northern boundary of the Himalayan orogenic belt in South Tibet, juxtaposing the Gangdese arc or Xigaze forearc basin to the north and the Tethyan Himalaya to the

* Corresponding author at: School of Earth Sciences, University of Melbourne, Melbourne 3010, Victoria, Australia.
E-mail address: guangwei.li@unimelb.edu.au (G. Li).

https://doi.org/10.1016/j.gr.2018.06.006
1342-937X/

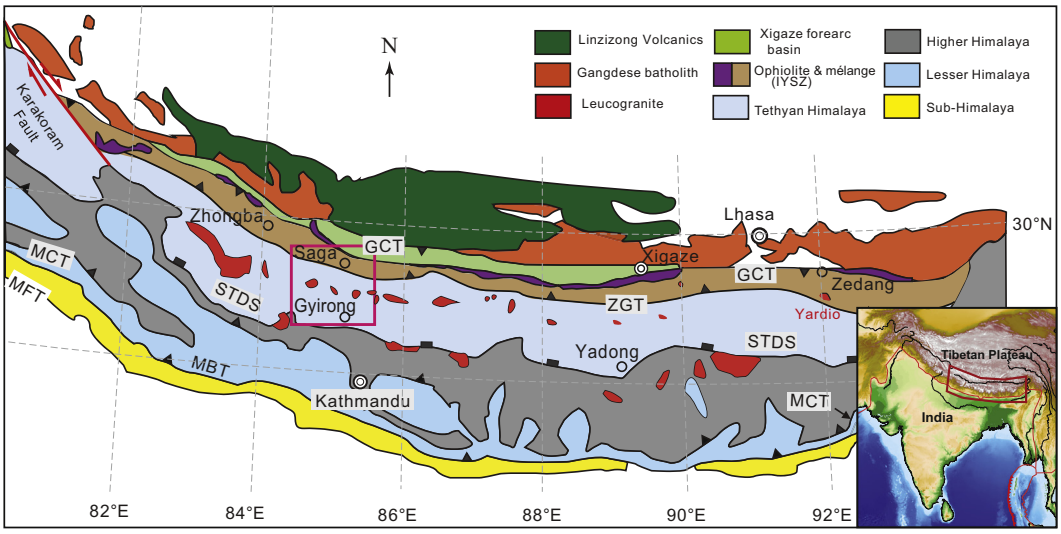

Fig. 1. Simplified geological map of southern Tibet showing study area (Saga-Gyirong). GCT - Great Counter Thrust; IYSZ - Indus-Yarlung Suture zone; MCT - Main Central Thrust; MBT - Main Boundary Thrust; MFT - Main Front Thrust; STDS - South Tibet Detachment System; ZGT - Zhongba-Gyanze Thrust. (Modified from Pan et al. (2004).)

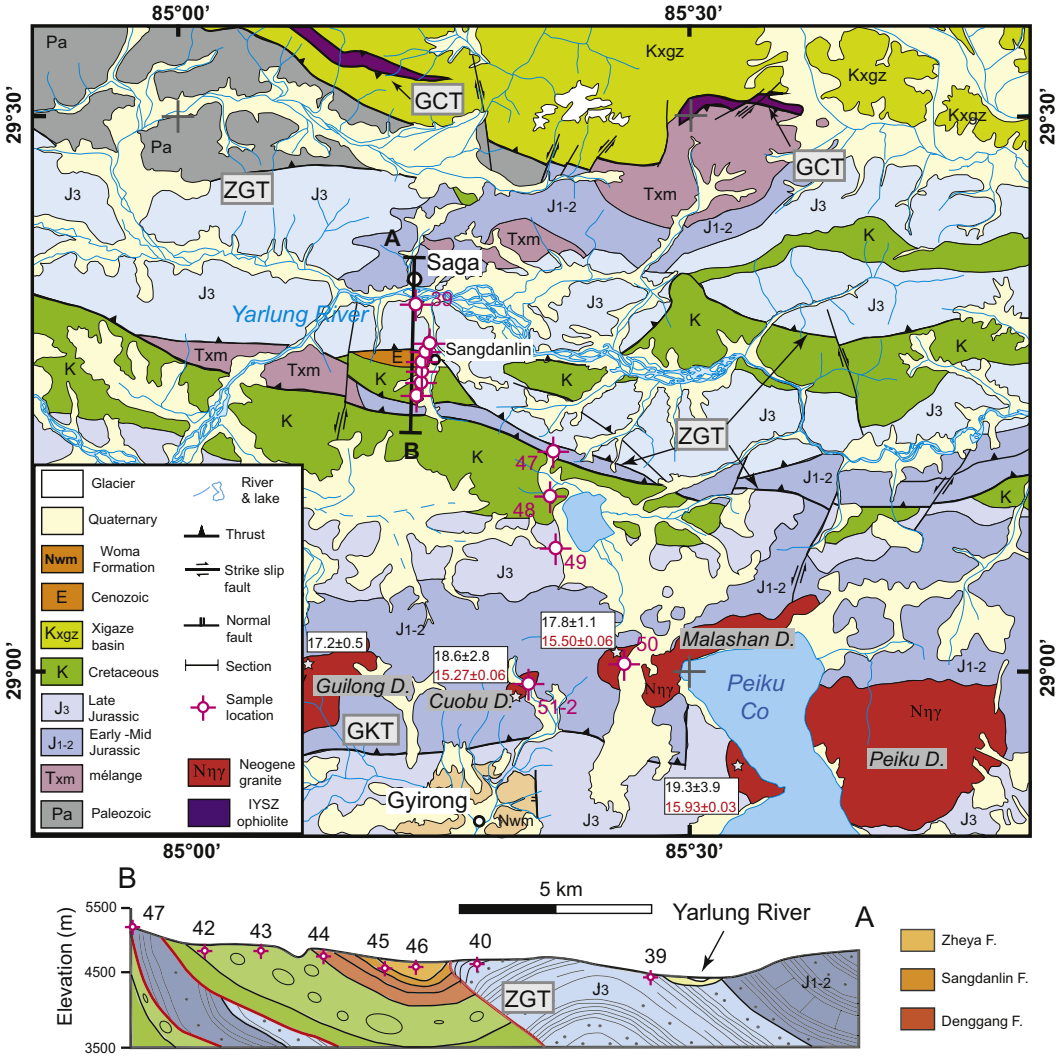

Fig. 2. A. Geological map of Saga region with sample locations. Crystallization and cooling ages of the Neogene dome leucogranites are listed; zircon U-Pb ages in black and mica ^{40}Ar-^{39}Ar ages in red in the box (Aoya et al., 2005; Kawakami et al., 2007; Shen et al., 2016). B. Cross section of Sangdanlin area with sample locations. GKT - Gamba-Kangma Thrust; F. - Formation.

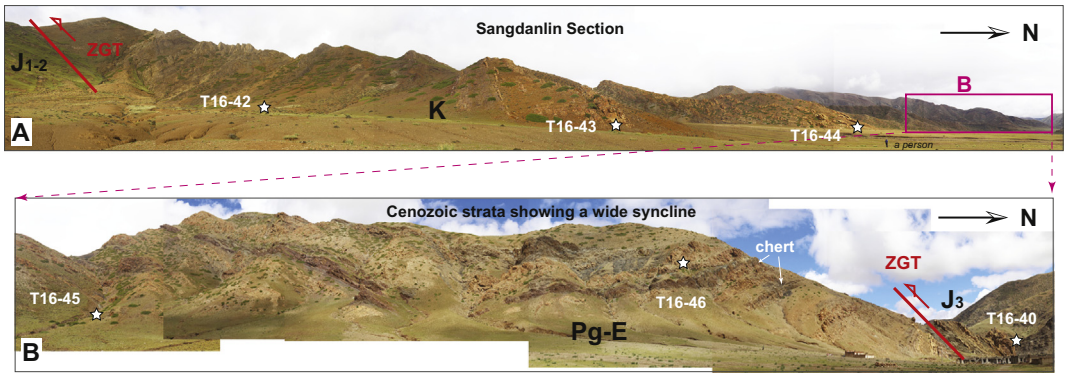

Fig. 3. Field features and lithologies of the Sangdanlin basin bounded by the ZGT. A. southern section showing Cretaceous sequences with sample locations. B. northern section of Cenozoic sequences showing a gentle wide syncline with sample locations.

south. The detailed boundaries between these geological units were strongly modified by the Late Oligocene north-dipping Gangdese Thrust (Yin et al., 1999) and Early Miocene south-dipping Great Counter Thrust (GCT, Ding et al., 2005; Murphy and Yin, 2003; Quidelleur et al., 1997) (Fig. 1). The Gangdese Arc, located along the southern margin of the Asian plate (Lhasa terrane), is composed of the Late Triassic to Cenozoic granitoids and volcanics series (e.g. Ji et al., 2009; Zhang et al., 2010; Zhu et al., 2011, 2013). To the south, the Xigaze forearc basin mainly consists of Early Cretaceous turbidites with foraminifera limestones and Late Cretaceous-Eocene shallow marine strata (e.g. An et al., 2014; Orme et al., 2014; Wang et al., 2012). The IYSZ, representing the boundary between Indian and Asian plates, includes ophiolite bodies and accretionary complexes. These Early Cretaceous ophiolites formed in a supra-subduction zone (or hyper-extended forearc) setting (Hébert et al., 2012; Maffione et al., 2015). The accretionary complexes consisting of serpentinite-matrix mélange and sedimentary-matrix mélange with preserved trench or wedge-top basins (Ding et al., 2005; DeCelles et al., 2014; Li et al., 2015b), were formed during the Cretaceous as a result of northward subduction of Neo-Tethyan oceanic lithosphere (Cai et al., 2012; Chen et al., 1984; Wang et al., 2017; Ziabrev et al., 2003). The Tethyan Himalaya, representing the Indian passive continental margin, is separated from the IYSZ by the Paleocene-Eocene Zhongba-Gyangze Thrust (ZGT) to the north (Ding et al., 2005; Ratschbacher et al., 1994; Wang et al., 2017; Fig. 1). It mainly consists of Paleozoic-Mesozoic shallow marine to deepwater sedimentary units, with sporadic Cenozoic basin (e.g. DeCelles et al., 2014; Ding et al., 2005; Li et al., 2010; Liu and Einsele, 1994). The Greater Himalaya, situated further south (Fig. 1), mainly consists of Proterozoic-Paleozoic high-grade metamorphosed metasedimentary rocks intruded by Paleozoic-Cenozoic granites, and Proterozoic–Paleozoic metasedimentary rocks (e.g. McQuarrie et al., 2013; Parrish and Hodges, 1996). The Lesser Himalaya mainly consists of Permian to Cretaceous strata, similar to those in the Tethyan Himalayan sequences (e.g. Yin, 2006).

The study region, located in the Saga-Gyirong area, southwest Tibet (Figs. 1 and 2), includes the Sangdanlin section within the sedimentary-matrix mélange and northern Tethyan Himalaya. The late Mesozoic-Cenozoic sedimentary sequences in Sangdanlin was deposited as a northern Indian passive margin sequence and forms a tilted, wide asymmetric syncline, located entirely within the ZGT zone. Its north flank, buried beneath the Late Jurassic sedimentary sequence, is cut by the

Table 1
Zircon (U-Th)/He data for the Sangdanlin and northern Tethyan Himalaya in this study.

Sample no.	^{4}He (ncc)	Mass (mg)	Mean (FT)	U (ppm)	Th (ppm)	Th/U	[eU] (ppm)	Corr. age (Ma)	Error (±2σ)	Grain length (μm)	Grain with (μm)	Weighted mean age (Ma)
Zircon												
T16-39	10.642	0.0088	0.81	418.3	336.3	0.80	497.3	**20.0**	**2.4**	218.1	120.3	
T16-39	9.108	0.0072	0.78	299.3	393.3	1.31	391.8	**26.3**	**3.2**	232.2	98.5	
T16-39	6.762	0.0076	0.79	338.8	216.9	0.64	389.8	**18.7**	**2.4**	237.6	99.7	
T16-39	2.239	0.0037	0.72	176.6	111.9	0.63	202.9	**24.2**	**3.0**	205.6	72.5	**22.1 ± 3.8**
T16-40	14.114	0.0080	0.79	616.0	630.7	1.02	764.2	**19.1**	**2.4**	233.5	104.1	
T16-40	7.397	0.0081	0.81	317.2	143.5	0.45	351.0	**21.4**	**2.6**	220.7	111.7	
T16-40	*5.957*	*0.0096*	*0.82*	*264.3*	*199.1*	*0.75*	*311.1*	*16.3*	*2.0*	*234.0*	*118.5*	
T16-40	*21.380*	*0.0070*	*0.78*	*619.2*	*356.1*	*0.58*	*702.9*	*35.8*	*4.4*	*235.2*	*95.0*	**20.7 ± 1.9**
T16-43	1.853	0.0084	0.81	60.6	70.2	1.16	77.1	**23.5**	**3.0**	196.2	136.2	
T16-43	8.309	0.0095	0.80	336.5	121.4	0.36	365.1	**19.6**	**2.4**	275.4	100.5	
T16-43	2.685	0.0038	0.74	248.5	212.5	0.86	298.4	**19.4**	**2.4**	163.2	92.5	
T16-43	*4.596*	*0.0063*	*0.79*	*728.3*	*548.0*	*0.75*	*857.1*	*7.0*	*0.8*	*188.2*	*112.7*	**20.5 ± 1.5**
T16-45	*3.750*	*0.0032*	*0.74*	*876.2*	*44.7*	*0.05*	*886.7*	*10.7*	*1.4*	*154.7*	*87.7*	
T16-45	18.387	0.0069	0.80	1077.8	433.0	0.40	1179.5	**18.4**	**2.2**	191.2	119.7	
T16-45	11.586	0.0090	0.80	361.8	138.7	0.38	394.4	**26.8**	**3.4**	245.5	107.6	**22.6 ± 4.2**
T16-47	4.402	0.0067	0.78	195.8	155.3	0.79	232.3	**23.0**	**2.8**	239.9	91.5	
T16-47	9.957	0.0041	0.75	847.1	696.5	0.82	1010.8	**19.5**	**2.4**	173.0	91.5	
T16-47	2.008	0.0071	0.78	106.0	50.8	0.48	118.0	**19.7**	**2.4**	258.1	88.7	**20.5 ± 1.5**
T16-48	23.780	0.0044	0.76	1202.7	607.7	0.51	1345.5	**32.9**	**4.0**	182.7	89.9	
T16-48	15.742	0.0142	0.83	247.6	129.6	0.52	278.1	**32.7**	**4.0**	293.2	122.3	**32.8 ± 2.9**
T16-49	4.330	0.0052	0.75	163.6	109.1	0.67	189.2	**35.8**	**4.4**	229.8	81.3	
T16-49	4.285	0.0078	0.80	101.4	91.1	0.90	122.8	**36.6**	**4.6**	232.5	103.3	
T16-49	*2.153*	*0.0038*	*0.74*	*289.5*	*113.5*	*0.39*	*316.2*	*14.9*	*1.8*	*176.9*	*83.4*	
T16-49	*10.213*	*0.0089*	*0.80*	*140.5*	*54.0*	*0.38*	*153.2*	*61.3*	*7.6*	*253.0*	*103.9*	**36.2 ± 3.2**

Note: Bold numbers represent corrected single grain ages and corresponding errors; italic grains were not used for calculating weighted mean ages because of effect of parent isotope zonation (Anderson et al., 2017) or possibly He trapped in fluid inclusions (Danišík et al., 2017).

ZGT (Figs. 2B, 3). The section is preserved as a successive Late Cretaceous-Early Eocene sedimentary sequence, divided into three formations. These include the upper Cretaceous Denggang/or Zongzhuo Formation (Fm.), Paleocene Sangdanlin Fm. and Paleocene-Lower Eocene Zheya Fm. The Denggang/Zongzhuo Fm. is mainly characterized by quartzarenitic turbidites with siliceous shale and chert, which is overlain by red chert, siliceous shale, and interbedded with quartzarenite of the Sangdanlin Fm. The Sangdanlin Fm. records the pivotal transition from Indian-derived strata to a mainly Asian-derived volcano-plutonic sequence, representing the initial India-Asia collision at ~60 Ma (DeCelles et al., 2014; Hu et al., 2015; Wu et al., 2014). The overlying Zheya Fm. is composed of dark grey siliceous shale and volcano-plutonic clastic turbidites with pebbly sandstone, characteristic of the uppermost strata (DeCelles et al., 2014; Ding et al., 2005; Hu et al., 2015; Wang et al., 2011). The sedimentary-matrix mélange, surrounding the Sangdanlin sequences, is mainly comprised of blocks of Triassic-Cenozoic northern Indian continental (Tethyan Himalayan) strata (Fig. 2; Cai et al., 2012; Li et al., 2015b; Wang et al., 2017). Further south, the northern Tethyan Himalayan sequence was intruded by Cenozoic leucogranites, which formed several domes (e.g. Peiku, Malashan, Cuobu and Guilong domes), bounded by the ZGT to the north and separated by the Early Miocene Gyirong-Kangmar Thrust (GKT; Lee et al., 2000) from the southern Tethyan Himalaya to the south (Fig. 2). The sedimentary succession in the northern Tethyan Himalaya mainly comprises sandstone, limestone, and shale with weak deformation and metamorphism. The domes form the western parts of the North Himalayan Gneiss Domes (NHGD; e.g. Lee et al., 2004; Zeng et al., 2011). These intrusions formed between ~19 and 17 Ma, with a consistent biotite $^{40}Ar/^{39}Ar$ cooling age of ~15 Ma (Aoya et al., 2005; Kawakami et al., 2007; Shen et al., 2016). Catchments for the Yarlung River and its tributaries cover the most of the study area (Fig. 2).

3. Samples and methods

Eight Late Jurassic to Eocene sandstones (T16-39, -40, -42–47; Figs. 2, 3) were collected along the NS transect A-B (GPS: E85.235, N29.313 to E85.357, N29.189) from the sedimentary-matrix mélange of the IYSZ in Sangdanlin. A further four samples (two sandstones: T16-48–49; two granites: T16-50, -51-2) were collected from the northern Tethyan Himalaya (Fig. 2). Sandstone sample T16-48 was taken from the Cretaceous Jiabula Formation, while sample T16-49 is from the Late Jurassic Weimei Formation in the Tethyan Himalaya (Fig. 2A). Granitic sample T16-50 is from the Early Miocene leucogranite of the Malashan dome, while sample T16-51-2 is from the Cuobu dome (Fig. 2A).

Samples were crushed and ground and processed by conventional heavy liquid and magnetic mineral separation techniques, to concentrate zircon and apatite grains. Low temperature thermochronology (AFT and ZHe) analyses were conducted in the School of Earth Sciences, University of Melbourne. Detailed information of these analytical procedures essentially followed descriptions in Gleadow et al. (2015), which are described in the Supplementary material. Two fine-grained sandstones (T16-48 and -49) from the northern Tethyan Himalaya did not yield suitable apatite for AFT analysis.

4. Results

ZHe and AFT ages for all samples analysed are significantly younger than their corresponding host stratigraphic/crystallization ages and P (χ^2) values (from 20% to 54%) of AFT ages for sandstones are much higher than 5% (Tables 1 and 2). Thus, the sandstone samples are considered to be fully reset thermally post-deposition with respect to the relatively higher ZHe closure temperature (>~180 °C, Reiners, 2005). In samples with both ZHe and AFT data, the latter ages are generally younger.

Table 2
Apatite fission track data for the Sangdanlin and northern Tethyan Himalaya, southwest Tibet.

^{0248}-Sample no.	Sample information			Age results									Track length and Dpar results						Mean Dpar (range) (μm)
	Lithology	Locality (°E/°N)	Elevation (m)	No. of grains (n)	Spontaneous tracks		Pooled[a] ^{238}U (ppm)	Pooled age[b] (Ma ± 1SD)			P (χ2)[c] (%)	Dispersion (%)	Central age[d] (Ma ± 1SD)			Non-projected[e] mean (μm ± 1SD)			Projected[f] mean (μm ± 1SD)			No. (n)	
					No. (n)	Density (10^5 cm^{-2})																
T16-39	Sandstone	85.235/29.313	4482	20	84	0.583	26.97	9.9	±	1.1	20	0	10.7	±	1.2	13.2	±	2.1	14.2	±	1.4	109	1.91 (1.6–2.4)
T16-40	Sandstone	85.257/29.266	4546	24	85	0.955	19.54	9.7	±	1.3	21	0	10.3	±	1.1	14.1	±	1.5	14.8	±	1.1	89	2.1 (1.6–2.7)
T16-42	Sandstone	85.247/29.221	4693	24	29	0.403	6.49	11.5	±	0.9	45	0	12.2	±	2.3	13.7	±	1.5	14.6	±	1.1	78	1.7 (1.4–2.1)
T16-43	Sandstone	85.244/29.230	4658	17	64	0.149	28.60	10.9	±	1.3	54	0	11.7	±	1.6	13.1	±	1.9	14.1	±	1.3	102	1.9 (1.5–2.5)
T16-44	Sandstone	85.251/29.246	4596	22	116	1.838	41.43	8.8	±	1.2	34	0	9.5	±	0.9	13.9	±	1.3	14.7	±	0.9	36	2.0 (1.3–2.8)
T16-45	Sandstone	85.252/29.259	4587	19	96	1.401	19.50	12.5	±	2.0	31	0	13.6	±	2.1	13.7	±	1.7	14.7	±	1.1	64	2.0 (1.8–2.3)
T16-46	Sandstone	85.253/29.261	4583	18	99	1.079	20.20	10.7	±	1.3	30	0	11.4	±	1.4	13.5	±	1.7	14.2	±	1.2	48	2.1 (1.5–2.9)
T16-47	Sandstone	85.357/29.189	4739	24	48	1.033	20.33	9.5	±	1.5	41	0	10.9	±	1.6	13.8	±	1.7	14.7	±	1.2	34	1.9 (1.2–2.6)
T16-50	Granite	85.439/28.975	4692	25	65	0.674	18.72	6.5	±	0.7	48	0	7.2	±	0.9	13.4	±	1.6	14.4	±	1.1	110	1.6 (1.4–1.9)
T16-51-2	Granite	85.304/28.954	4895	34	1488	7.105	145.30	9.8	±	0.4	34	0	9.6	±	0.4	13.6	±	1.6	14.5	±	1.1	184	1.5 (1.3–1.7)

[a] Pooled uranium content of all grains measured by LA-ICP-MS.
[b] Pooled AFT ages of all grains.
[c] P-value of χ^2 for (n − 1) degrees of freedom (Galbraith, 1981).
[d] Central age calculated using the RadialPlotter program of Vermeesch (2009).
[e] Lengths measured after ^{252}Cf irradiation.
[f] c-Axis projected mean track length after Ketcham et al. (2007).

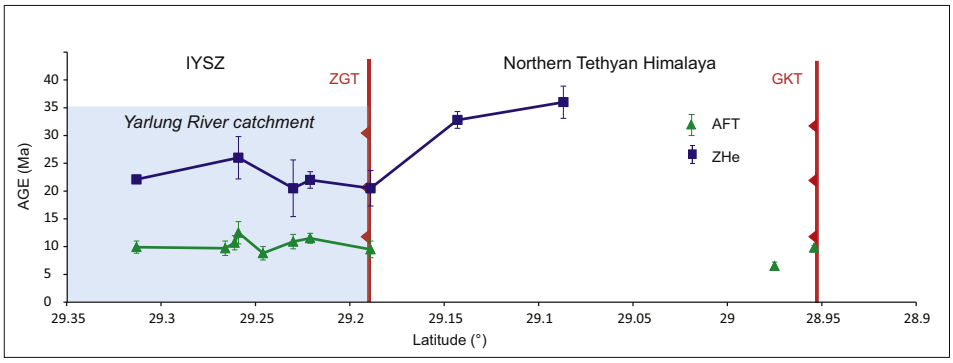

Fig. 4. Low-thermochronology ages (AFT and weighted mean ZHe; see Tables 1 and 2) versus latitude plots along the sampling transect A–B marked in Fig. 2, including the IYSZ and northern Tethyan Himalaya.

4.1. ZHe data

ZHe data from seven samples (3–4 single grain analyses per sample) were analysed (Table 1). Five sandstone samples (T16-39, -40,-43, -45 and -47) from the mélange fault zone yielded consistent Late-Oligocene-Early Miocene ZHe ages, mainly ranging from 18.4 to 26.8 Ma, which are substantially younger than their Late Jurassic to Early Eocene depositional ages. Four single grain analyses fall outside this age range. However, these ages do not appear to correlate with their eU content or grain size (e.g. Guenther et al., 2013, Table 1; Fig. S1 in the Supplementary material), but the effect of parent isotope zonation may be an unknown factor at play in these grains (Anderson et al., 2017) or possibly He trapped in fluid inclusions (Danišík et al., 2017). In two sandstone samples from the northern Tethyan Himalaya, four out of six grains mainly yielded earliest Oligocene to latest Eocene ZHe ages ranging from ~32.8 ± 2.9 to 36.2 ± 3.2 Ma, much younger than their depositional ages of Late Jurassic and Early Cretaceous, respectively, with two yielding apparent age outliers (Table 1; Fig. 4), possibly due to factor/s outlined above.

4.2. AFT data

Eight samples (T16-39–47) from the mélange (mainly the Sangdanlin section) within the ZGT zone in Saga yielded consistent Middle Miocene ages, ranging from 8.8 ± 1.2 Ma to 12.5 ± 2.0 Ma, including sample T16-47 with an age of 9.5 ± 1.5 Ma, collected from the highest elevation (~4800 m) and located on the southern margin of the ZGT zone. These samples contain relatively long non-projected track lengths, with mean values ~13–14 μm (Table 2). Two granite samples from Miocene domes in the northern Tethyan Himalaya yielded Late Miocene ages of 6.5 ± 0.7 Ma and 9.8 ± 0.4 Ma and relatively long non-projected track mean lengths of 13.4 ± 1.6 and 13.6 ± 1.6 μm, respectively (Table 2; Fig. 4). This suggests that all these samples experienced relatively fast cooling following reheating or crystallization (Gleadow et al., 1986).

4.3. Thermal modelling and interpretations

Thermal history modelling from 10 sample was carried out using HeFTy (Ketcham et al., 2007), together with other geological constraints. For AFT data, the multi-kinetic annealing model of Ketcham et al. (2007) was applied, using Dpar value as a kinetic parameter; while the helium diffusion model of Guenther et al. (2013) was used for single grain ZHe data within each sample. Further, the present-day surface temperature was set at 10 ± 5 °C. For those samples without accompanying ZHe analyses from the mélange zone (T16-42, -44 and -46), the ZHe data from their closest neighboring samples were also used as constraints (but with larger uncertainties). Two granite samples (T16-50 and -51-2) from the NHGD were constrained by their biotite $^{40}Ar/^{39}Ar$ cooling ages (Aoya et al., 2005; Kawakami et al., 2007). Other details of parameters for HeFTy followed the principles presented by G.-W. Li et al. (2017).

4.3.1. Mélange zone of IYSZ including Sangdanlin area

Thermal history modelling results of eight samples from the IYSZ mélang zone (including 5 samples from the Sangdanlin section), show a mostly consistent thermal history pattern, indicating relatively slow Early Miocene cooling followed by a rapid cooling episode commencing between ~12 ± 2 and 6 ± 2 Ma, from 120 to 150 °C. All samples passed through the AFT partial annealing zone (60–120 °C) in the Middle-Late Miocene time, followed by relatively slow cooling to the surface (Fig. 5).

4.3.2. Northern Tethyan Himalaya

Two granite samples from the NHGD were modelled in combination with AFT and $^{40}Ar/^{39}Ar$ data, yielded a similar thermal history. These results are characterized by relatively rapid cooling from 350 to 150 °C within ~3 ± 2 Ma, commencing in the Middle Miocene (between ~15 and 12 Ma), followed by relatively slow Late Miocene to Recent cooling through the AFT partial annealing zone (Fig. 5).

5. Discussion

5.1. Cooling history of IYSZ and Tethyan Himalaya

As described above, samples reported in this study cover the IYSZ and northern part of the Tethyan Himalaya in southwest Tibet. Samples from the two tectonic units clearly show different themochronological age and cooling/exhumation patterns.

5.1.1. IYSZ

Samples from the IYSZ mélange near Saga (e.g. Mesozoic sedimentary matrix and Cenozoic Sangdanlin sequence), show a similar history of rapid Middle-Late Miocene cooling history following a period of Early Miocene quiescence in a relative higher temperature zone (Fig. 5). This suggests that all units in the mélange underwent a similar heating and cooling history, which is here related to burial and exhumation, respectively. In the Early Miocene, the mélange resided in a >120 °C temperature zone. Considering the present day geothermal gradient in the region (~30 °C/km; Hu et al., 2000), we estimate that ~4 km thickness of overlying possible Late Eocene section and/or a thrust sheet, would have been removed, leaving only pre-Middle Eocene (>42 Ma) strata preserved (e.g. Ding et al., 2005; Wang et al., 2011). Based on a thermal history study, G.-W. Li et al. (2017) and S. Li et al. (2017) proposed that the sedimentation in the Xigaze basin (located immediately north side

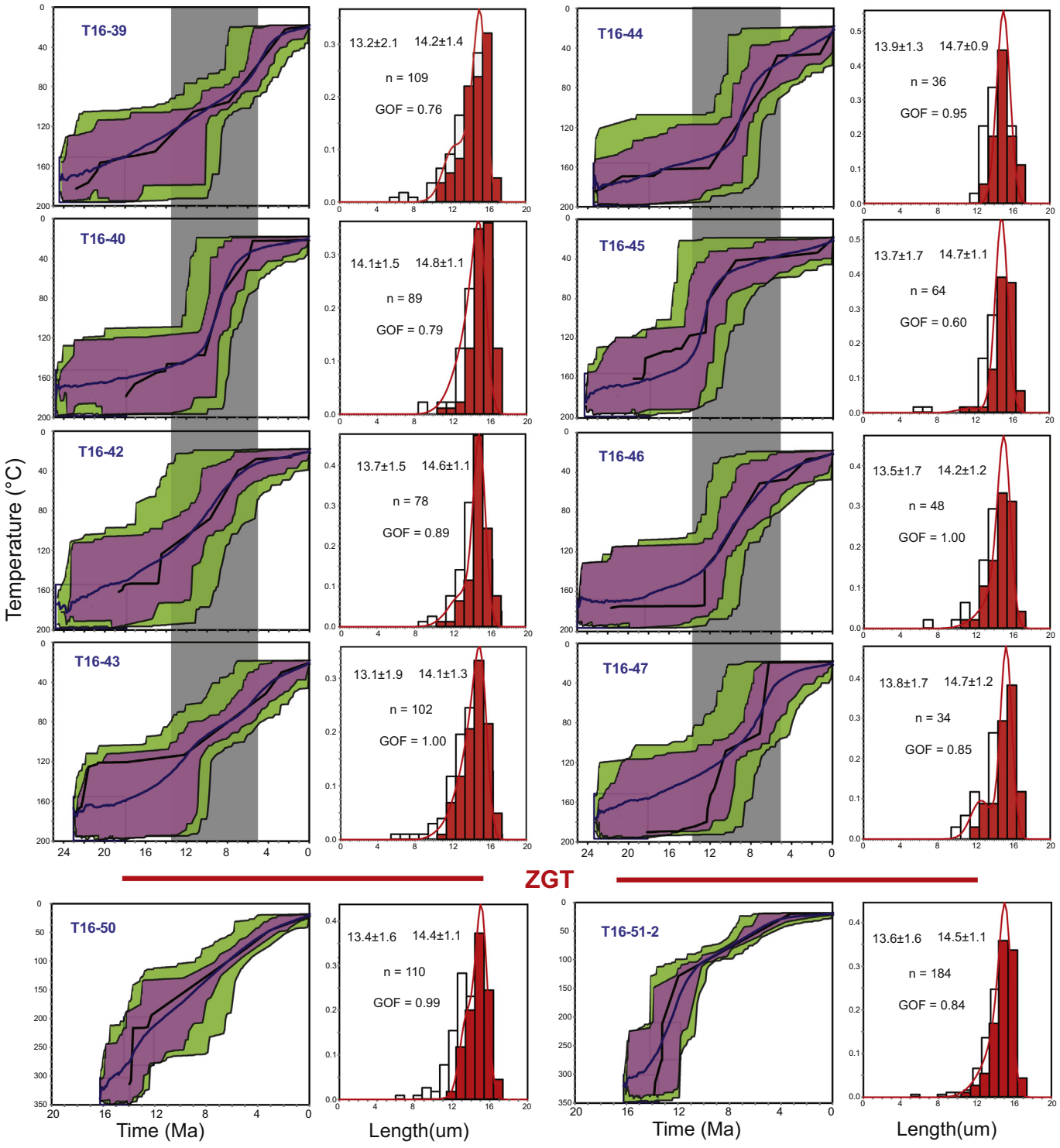

Fig. 5. Thermal history modelling based on AFT, ZHe, Ar-Ar data of samples using HeFTy. Models use the AFT annealing model of Ketcham et al. (2007) and the radiation damage accumulation and annealing zircon He diffusion model (Guenther et al., 2013). Left panel: purple envelopes indicate 'good' thermal paths GOF = goodness of fit (GOF > 0.55) and green envelopes indicate 'acceptable' thermal paths (GOF > 0.05). Boxes indicate constraints used for modelling (see text). The best-fit thermal path for each sample is shown as a heavy black line. Right panel: length distribution panel; the best-fit thermal path length distribution pattern (the red curve) is compared with the measured length (white histogram) and C-projected length (red histogram).

of the IYSZ) probably lasted up to latest Eocene time (~35 Ma). This suggests that during the Eocene post-collisional sedimentary (foreland) sequences developed across the region. Further, the GCT was active regionally during the Early Miocene (Yin, 2006), but evidence is only preserved further north of Saga (Figs. 1, 2 and 6), rather than in the actual study area (Fig. 2). However, the GCT in areas to the east involves the IYSZ mélange, and even the northern Tethyan Himalaya units (Yin, 2006; Li et al., 2015c). There is a slight reverse trace (dipping north) preserved at the northern flank of the Cenozoic sequence in the Sangdanlin syncline (Figs. 2B and 3B), although the main fault panels dip to the

north in the study area. Hence, we propose that the GCT also impacted the IYSZ mélange in Saga, and probably thrust a 'Tethyan Himalaya' sheet over the Sangdanlin section, however, direct evidence has since been almost entirely removed. Furthermore, based on numerical simulations, Tremblay et al. (2015) proposed that since the Late Miocene the Yarlung River drainage reorganization would have driven the pronounced reduction in the exhumation rate in southern Tibet, an observation consistent with our data. Thus, we conclude that the Middle-Late Miocene fast cooling is mainly related to post-GCT thrust erosion due to incision by the Yarlung River (Fig. 2). This is consistent with the cooling history previously described from other areas to the east, along the current Yarlung River (e.g. Carrapa et al., 2014, 2017; Li et al., 2015c; G.-W. Li et al., 2017; Fig. 6).

5.1.2. Northern Tethyan Himalaya

Due to absence of apatite, the Mesozoic sequences in the northern Tethyan Himalaya, only yielded two Late Eocene-Early Oligocene ZHe ages. These indicate that the earlier cooling/exhumation episode of the Tethyan Himalaya, is older than that of the IYSZ. This cooling is comparable with findings reported from other areas within the Tethyan Himalaya (e.g. Xigaze and Zedang; Carrapa et al., 2014; Li et al., 2015c; Fig. 6). Based on the detrital thermochronology data from the Gyirong basin in the Tethyan Himalaya, further south of the study area, Shen et al. (2016) reported an older prominent age group of ~41–37 Ma. Hence, this widespread Eocene cooling episode relates to activity of the Tethyan Himalaya fold-thrust zone (Yin and Harrison, 2000; Li et al., 2015c), which has not been overprinted by later tectonic activity, e.g. by GCT movement. Two granite samples from the NHGD experienced a pronounced Middle Miocene rapid cooling/exhumation episode (Fig. 5), which is consistent with that of the Yardoi dome to the east (Fig. 1), Zedang area (Li et al., 2015c; Fig. 6). This cooling episode is probably related to doming and formation of the NHGD in the northern Tethyan Himalaya. Further south, a group of detrital AFT apparent ages at ~15–18 Ma was interpreted as indicating a rapid Early Miocene exhumation episode in the Tethyan Himalaya (Shen et al., 2016). However, given that no length data or thermal history modelling were presented, the precise timing of cooling/exhumation in that region requires further investigation.

Generally, the earlier cooling/exhumation recorded in the Tethyan Himalaya (Fig. 6), is linked to activity of the Tethyan Himalaya fold-thrust zone. The later Miocene scenarios were mainly controlled by regional formation of the NHGD and rifting (Li et al., 2015c). However, there are still only sporadic data published for the Tethyan Himalaya (Fig. 6), thus details of the pre-Oligocene exhumation history are still not clear.

5.2. Pronounced Miocene cooling/exhumation along the Yarlung River in South Tibet

The latest Oligocene-Early Miocene Kailas Conglomerate along the north side of Indus-Yarlung ophiolites for >1000 km provides evidence that the Yarlung River and its tributaries have flowed along the IYSZ, partially across southern Gangdese batholith, Xigaze forearc arc in South Tibet, since at least Early Miocene time (Figs. 6, 7; e.g. Wang et al., 2013; S. Li et al., 2017). Except for the pre- Middle Eocene rapid cooling/exhumation recorded in the southern Gangdese (e.g. Ge et al., 2017; Li et al., 2016) and Xigaze forearc basin (G.-W. Li et al., 2017), the region experienced a widespread and pronounced Early to Late Miocene fast cooling episode (e.g. Carrapa et al., 2014; Dai et al., 2013; Li et al., 2016; G.-W. Li et al., 2017; Ge et al., 2017; Orme, 2017). In this region (e.g. southern Gangdese batholith, Xigaze forearc basin and IYSZ), the late Oligocene Gangdese Thrust and Early Miocene GCT are major fault systems (e.g. Yin, 2006; Quidelleur et al., 1997), which may have exerted a fundamental control on regional Early Miocene cooling. Regional uplift was also suggested to have resulted from crustal flexure due to the effect of thrust sheet overloading (Wang et al., 2015) or the Indian slab rollback (Shen et al., 2016) in the Early Miocene. However, uplift cannot directly trigger large-scale cooling without erosion. The record of Early Miocene cooling is mainly localised to a narrow zone, including the southern boundary of the Gangdese batholith (Li et al., 2016;Ge et al., 2017; Tremblay et al., 2015), and the Kailas Conglomerate belt (Carrapa et al., 2014), which are both located near fault planes of the Gangdese Thrust and GCT. The onset of the southern Gangdese batholith cooling youngs northwards, which is mainly attributed to headward incision of the Yarlung River tributaries (Fig. 7). In summary, regional Miocene cooling/exhumation episodes were related to activity of the Gangdese Thrust and GCT, or due to the combined effect of flexural bending coupled with erosion by the Yarlung River and its tributaries (e.g. Carrapa et al., 2014; Wang et al., 2015; Li et al., 2016; Tremblay et al., 2015).

Within the IYSZ, thermal history modelling of the Sangdanlin section in Saga indicates that it has experienced relatively fast post-Middle

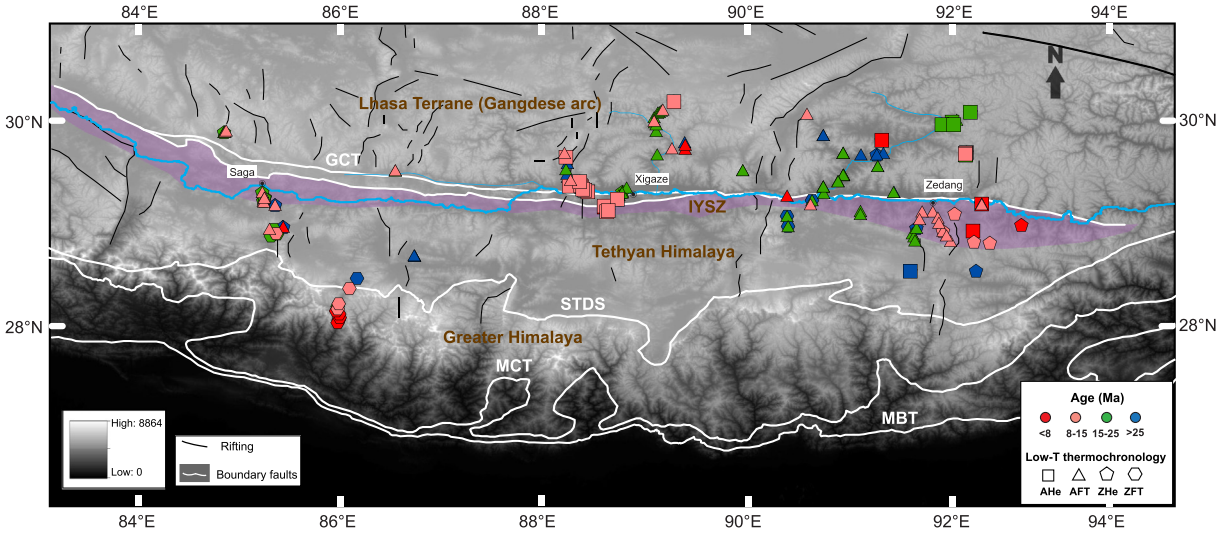

Fig. 6. Low-T thermochronology data from the southern Tibet, including Gangdese arc, IYSZ and Tethyan Himalaya. Abbreviations as for Fig. 1.
Data cited are from Dai et al. (2013), Ge et al. (2017), Li et al. (2015a,c, 2016), G.-W. Li et al. (2017), Orme (2017); Shen et al. (2016) and references therein.

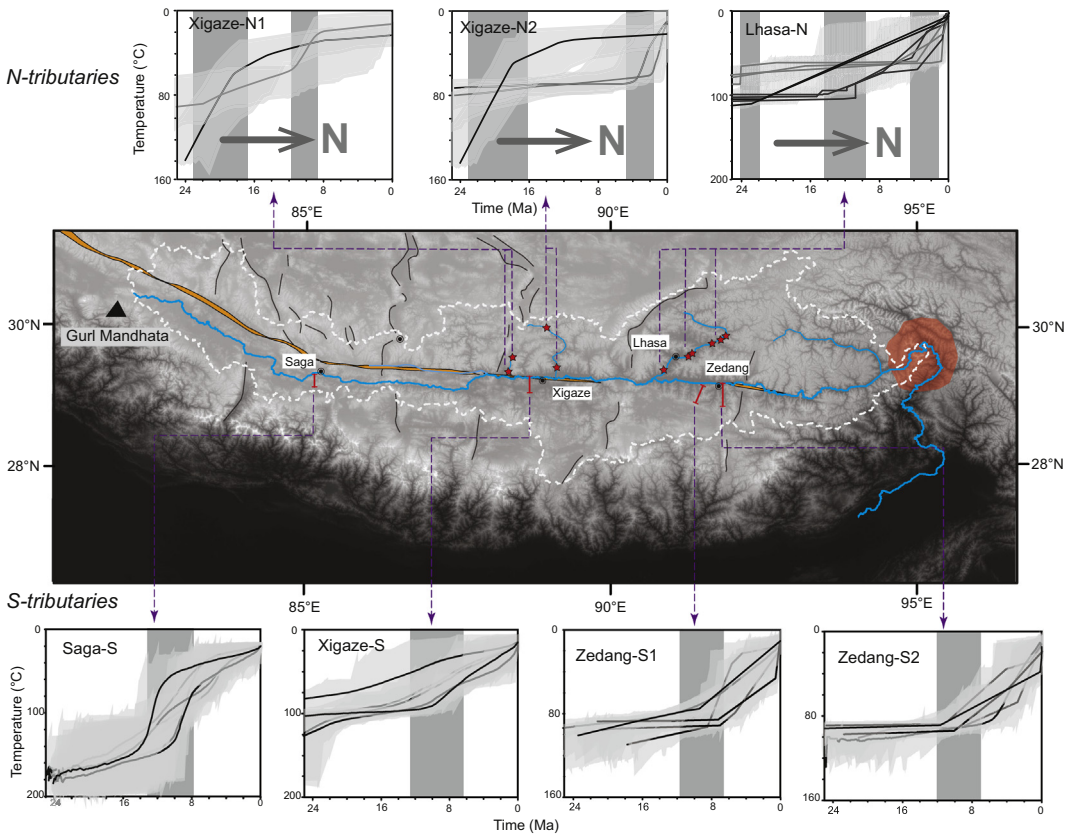

Fig. 7. Cooling history of Yarlung River bedrock tributaries. Tributaries on the north side show progressive cooling episodes through the Miocene (data from Ge et al., 2017; Li et al., 2016), while those on the south side show a more pronounced, common cooling episode at ~10 ± 3 Ma (data from Li et al., 2015c; G.-W. Li et al., 2017 and this study). The red shaded zone represents the Grand Tsangpo Gorge in the Eastern Himalaya Syntax.

Miocene cooling, consistent with the cooling history from the southern side of the Yarlung River in Xigaze and Zedang further east (Fig. 7). Taken together low-temperature thermochronology studies on tributaries of the Yarlung River, consistently show that in the northern tributaries a cooling episode commenced in the Early Miocene or earlier. As a result of headward incision the onset of cooling in these tributaries youngs upstream, to the north. However, a cooling episode of the southern tributaries clearly commenced in the Middle Miocene (~10 ± 3 Ma), implying post-GCT incision of the southern tributaries (Li et al., 2015c). To the east, the paleo-course of the Yarlung River (marked by the Kailas conglomerate) generally overlaps with the current course of the Yarlung River, while to the west it is offset significantly from the trunk of the present river course (Fig. 7). Furthermore, the Kailas conglomerate was strongly sheared and deformed within the GCT fault zone in Zedang to the east, and is currently preserved along the crest of the valley in the area (Xu et al., 2015). Thus, the current course of the Yarlung River was formed following cessation of the GCT movement. Hence, the Miocene GCT, parallel to the ancient river course, played an important role in the reorganization of the Yarlung River system (Fig. 6; Yin et al., 1999; Quidelleur et al., 1997).

Acknowledgements

This study benefited from financial support by Australian Research Council DECRA (Discovery Early Career Research Award, DE120102245) and China Geological Survey (No. 1212010818094) and Education Department of JiangXi Province, China (No. GJJ160776). The University of Melbourne Thermochronology Laboratory receives infrastructure support under the AuScope program of the National Collaborative Research Infrastructure Strategy (NCRIS). We thank Kai Cao and anonymous reviewer for their helpful suggestions for improving the manuscript and Editor Zemin Zhang for editorial handling. We are grateful to Abaz Alimanovic for assistance with ZHe analyses.

Appendix A. Supplementary data

Supplementary data to this article can be found online at https://doi.org/10.1016/j.gr.2018.06.006.

References

An, W., Hu, X., Garzanti, E., Boudagher-Fadel, M.K., Wang, J., Sun, G., 2014. Xigaze forearc basin revisited (South Tibet): provenance changes and origin of the Xigaze Ophiolite. Geological Society of America Bulletin 126 (11–12), 1595–1613.

Anderson, A., Hodges, K.V., van Soest, M.C., 2017. Empirical constraints on the effects of radiation damage on helium diffusion in zircon. Geochimica et Cosmochimica Acta 218, 308–322.

Aoya, M., Wallis, S.R., Terada, K., Lee, J., Kawakami, T., Wang, Y., Heizler, M., 2005. North-south extension in the Tibetan crust triggered by granite emplacement. Geology 33 (11), 853–856. https://doi.org/10.1130/G21806.1.

Cai, F., Ding, L., Leary, R.J., Wang, H.Q., Xu, Q., Zhang, L.Y., Yue, Y.H., 2012. Tectonostratigraphy and provenance of an accretionary complex within the Yarlung–Zangpo suture zone, southern Tibet: insights into subduction–accretion processes in the Neo-Tethys. Tectonophysics 574–575, 181–192.

Carrapa, B., Orme, D., DeCelles, P., Kapp, P., Cosca, M., Waldrip, R., 2014. Miocene burial and exhumation of the India-Asia collision zone in southern Tibet: response to slab dynamics and erosion. Geology 42 (5), 443–446. https://doi.org/10.1130/G35350.1.

Carrapa, B., bin Hassim, M.F., Kapp, P.A., DeCelles, P.G., Gehrels, G., 2017. Tectonic and erosional history of southern Tibet recorded by detrital chronological signatures along the Yarlung River drainage. Geological Society of America Bulletin 129 (5-6), 570–581.

Chen, G.M., Li, G.C., Qu, J.C., 1984. The mélanges and their tectonic significance in the Southern Xizang (Tibet). Himalaya Geology II: Part of Achievements in Geoscientific

Investigation of Sino-French Cooperation in the Himalayas in 1981. Geological Publishing House, Beijing, pp. 19–26 (edited, in Chinese with English abstract).
Dai, J., Wang, C., Hourigan, J., Li, Z., Zhuang, G., 2013. Exhumation history of the Gangdese Batholith, Southern Tibetan Plateau: evidence from Apatite and Zircon (U-Th)/He thermochronology. Journal of Geology 121 (2), 155–172.
Danišík, M., McInnes, B.I., Kirkland, C.L., McDonald, B.J., Evans, N.J., Becker, T., 2017. Seeing is believing: visualization of He distribution in zircon and implications for thermal history reconstruction on single crystals. Science Advances 3 (2), e1601121.
DeCelles, P., Kapp, P., Gehrels, G., Ding, L., 2014. Paleocene-Eocene foreland basin evolution in the Himalaya of southern Tibet and Nepal: implications for the age of initial India-Asia collision. Tectonics 33 (5), 824–849.
Ding, L., Kapp, P., Wan, X., 2005. Palaeocene–Eocene record of ophiolite obduction and initial India–Asia collision, south-central Tibet. Tectonics 24, TC3001. https://doi.org/10.1029/2004TC001729.
Galbraith, R.F., 1981. On statistical models for fission track counts. Journal of the International Association for Mathematical Geology 13 (6), 471–478. https://doi.org/10.1007/bf01034498.
Ge, Y.-K., Dai, J.-G., Wang, C.-S., Li, Y.-L., Xu, G.-Q., Danisik, M., 2017. Cenozoic thermotectonic evolution of the Gangdese batholith constrained by low-temperature thermochronology. Gondwana Research 41, 451–462. https://doi.org/10.1016/j.gr.2016.05.006.
Gleadow, A.J.W., Duddy, I.R., Green, P.F., Lovering, J.F., 1986. Confined fission track lengths in apatite – adiagnostic tool for thermal history analysis. Contributions to Mineralogy and Petrology 94, 405–415.
Gleadow, A., Harrison, M., Kohn, B., Lugo-Zazueta, R., Phillips, D., 2015. The Fish Canyon Tuff: a new look at an old low-temperature thermochronology standard. Earth and Planetary Science Letters 424, 95–108.
Guenther, W.R., Reiners, P.W., Ketcham, R.A., Nasdala, L., Giester, G., 2013. Helium diffusion in natural zircon: radiation damage, anisotropy, and the interpretation of zircon (U-Th)/He thermochronology. American Journal of Science 313 (3), 145–198.
Hébert, R., Bezard, R., Guilmette, C., Dostal, J., Wang, C.S., Liu, Z.F., 2012. The Indus-Yarlung Zangbo ophiolites from Nanga Parbat to Namche Barwa syntaxes, southern Tibet: first synthesis of petrology, geochemistry, and geochronology with incidences on geodynamic reconstructions of Neo-Tethys. Gondwana Research 22, 377–397.
Hu, S., He, L., Wang, J., 2000. Heat flow in the continental area of China: a new data set. Earth and Planetary Science Letters 179 (2), 407–419. https://doi.org/10.1016/s0012-821x(00)00126-6.
Hu, X., Garzanti, E., Moore, T., Raffi, I., 2015. Direct stratigraphic dating of India-Asia collision onset at the Selandian (middle Paleocene, 59±1 Ma). Geology 43 (10), 859–862.
Ji, W.Q., Wu, F.Y., Chung, S.L., Li, J.X., Liu, C.Z., 2009. Zircon U–Pb chronology and Hf isotopic constraints on the petrogenesis of Gangdese batholiths, southern Tibet. Chemical Geology 262, 229–245.
Kawakami, T., Aoya, M., Wallis, S.R., Lee, J., Terada, K., Wang, Y., Heizler, M., 2007. Contact metamorphism in the Malashan dome, North Himalayan gneiss domes, southern Tibet: an example of shallow extensional tectonics in the Tethys Himalaya. Journal of Metamorphic Geology 25, 831–853. https://doi.org/10.1111/j.1525-1314.2007.00731.x.
Ketcham, R.A., Carter, A., Donelick, R.A., Barbarand, J., Hurford, A.J., 2007. Improved measurement of fissiontrack annealing in apatite using C-axis projection. American Mineralogist 92, 789–798.
Lee, J., Hacker, B.R., Dinklage, W.S., Wang, Y., Gans, P., Calvert, A., Wan, J., Chen, W., Blythe, A.E., McClelland, W., 2000. Evolution of the Kangmar dome, southern Tibet: structural, petrologic, and thermochronologic constraints. Tectonics 19, 872–895.
Lee, J., Hacker, B.R., Wang, Y., 2004. Evolution of north Himalayan gneiss domes: structural and metamorphic studies in Mabja dome, southern Tibet. Journal of Structural Geology 26, 2297–2316. https://doi.org/10.1016/j.jsg.2004.02.013.
Li, G.-W., Liu, X.H., Pullen, A., Wei, L.J., Liu, X.B., Huang, F.X., Zhou, X.J., 2010. In-situ detrital zircon geochronology and Hf isotopic analyses from Upper Triassic. Earth and Planetary Science Letters 297, 461–470.
Li, G.-W., Kohn, B., Sandiford, M., Xu, Z., Wei, L., 2015a. Constraining the age of Liuqu Conglomerate, southern Tibet: implications for evolution of the India–Asia collision zone. Earth and Planetary Science Letters 426, 259–266.
Li, G.-W., Sandiford, M., Boger, S., Liu, X., Wei, L., 2015b. Provenance of the Upper Cretaceous to Lower Tertiary sedimentary relicts in the Renbu Melange Zone, within the Indus-Yarlung Suture Zone. The Journal of Geology 123 (1), 39–54. https://doi.org/10.1086/680207.
Li, G.-W., Tian, Y., Kohn, B.P., Sandiford, M., Xu, Z., Cai, Z., 2015c. Cenozoic low temperature cooling history of the Northern Tethyan Himalaya in Zedang, SE Tibet and its implications. Tectonophysics 643, 80–93.
Li, G.-W., Kohn, B., Sandiford, M., Xu, Z., Tian, Y., Seiler, C., 2016. Synorogenic morphotectonic evolution of the Gangdese batholith, South Tibet: insights from low-temperature thermochronology. Geochemistry, Geophysics, Geosystems 17 (1), 101–112.
Li, G.-W., Kohn, B., Sandiford, M., Xu, Z., 2017a. India-Asia convergence: insights from burial and exhumation of the Xigaze fore-arc basin, south Tibet. Journal of Geophysical Research - Solid Earth 122. https://doi.org/10.1002/2017JB014080.
Li, S., Ding, L., Xu, Q., Wang, H., Yue, Y., Baral, U., 2017b. The evolution of Yarlung Tsangpo River: constraints from the age and provenance of the Gangdese Conglomerates, southern Tibet. Gondwana Research 41, 249–266. https://doi.org/10.1016/j.gr.2015.05.010.
Liu, G., Einsele, G., 1994. Sedimentary history of the Tethyan basin in the Tibetan Himalayas. Geologische Rundschau 83, 32–61.
Maffione, M., van Hinsbergen, D.J.J., Koornneef, L.M.T., Guilmette, C., Hodges, K., Borneman, N., Huang, W., Ding, L., Kapp, P., 2015. Forearc hyperextension dismembered the South Tibetan ophiolites. Geology 43 (6), 475–478. https://doi.org/10.1130/G36472.1.
McQuarrie, N., Long, S.P., Tobgay, T., Nesbit, J.N., Gehrels, G., Ducea, M.N., 2013. Documenting basin scale, geometry and provenance through detrital geochemical data: lessons from the Neoproterozoic to Ordovician Lesser, Greater, and Tethyan Himalayan strata of Bhutan. Gondwana Research 23, 1491–1510. https://doi.org/10.1016/j.gr.2012.09.002.
Murphy, M., Yin, A., 2003. Structural evolution and sequence of thrusting in the Tethyan fold-thrust belt and Indus-Yalu suture zone, southwest Tibet. Geological Society of America Bulletin 115 (1), 21–34.
Orme, D.A., 2017. Burial and exhumation history of the Xigaze forearc basin, Yarlung suture zone, Tibet. Geoscience Frontiers https://doi.org/10.1016/j.gsf.2017.11.011.
Orme, D.A., Carrapa, B., Kapp, P., 2014. Sedimentology, provenance and geochronology of the upper Cretaceous–lower Eocene western Xigaze forearc basin, southern Tibet. Basin Research 27 (4), 387–411.
Pan, G., Ding, J., Yao, D., Wang, L. 2004. Geological map of Qinghai-Xizang (Tibet) Plateau and Adjacent Areas (1:1,500,000). Chengdu Institute of Geology and Mineral Resources, China Geological Survey. Chengdu Cartographic Publishing House.
Parrish, R., Hodges, K.V., 1996. Isotopic constraints on the age and provenance of the Lesser and Greater Himalayan sequences, Nepalese Himalaya. Geological Society of America Bulletin 108, 904–911.
Quidelleur, X., Grove, M., Lovera, O.M., Harrison, T.M., Yin, A., Ryerson, F.J., 1997. Thermal evolution and slip history of the Renbu Zedong Thrust, southeastern Tibet. Journal of Geophysical Research 102, 2659–2679.
Ratschbacher, L., Frisch, W., Liu, G., Chen, C., 1994. Distributed deformation in southern and western Tibet during and after the India–Asia collision. Journal of Geophysical Research 99, 19817–19945.
Reiners, P.W., 2005. Zircon (U-Th)/He thermochronometry. Reviews in Mineralogy and Geochemistry 58 (1), 151–179.
Rohrmann, A., Kapp, P., Carrapa, B., Reiners, P.W., Guynn, J., Ding, L., Heizler, M., 2012. Thermochronologic evidence for plateau formation in central Tibet by 45 Ma. Geology 40 (2), 187–190.
Shen, T., Wang, G., Leloup, P., van der Beek, P., Bernet, M., Cao, K., Wang, A., Liu, C., Zhang, K., 2016. Controls on Cenozoic exhumation of the Tethyan Himalaya from fission-track thermo-chronology and detrital zircon U-Pb geochronology in the Gyirong basin area, southern Tibet. Tectonics 35. https://doi.org/10.1002/2016TC004149.
Thiede, R.C., Ehlers, T.A., 2013. Large spatial and temporal variations in Himalayan denudation. Earth and Planetary Science Letters 371, 278–293.
Tremblay, M.M., Fox, M., Schmidt, J.L., Tripathy-Lang, A., Wielicki, M.M., Harrison, T.M., ... Shuster, D.L., 2015. Erosion in southern Tibet shut down at ~10 Ma due to enhanced rock uplift within the Himalaya. Proceedings of the National Academy of Sciences https://doi.org/10.1073/pnas.1515652112.
Vermeesch, P., 2009. RadialPlotter: a Java application for fission track, luminescence and other radial plots. Radiation Measurements 44 (4), 409–410.
Wang, J., Hu, X., Jansa, L., Huang, Z., 2011. Provenance of the Upper Cretaceous–Eocene deep-water sandstones in Sangdanlin, southern Tibet: constraints on the timing of initial India-Asia collision. The Journal of Geology 119 (3), 293–309.
Wang, C., Li, X., Liu, Z., Li, Y., Jansa, L., Dai, J., Wei, Y., 2012. Revision of the Cretaceous–Paleogene stratigraphic framework, facies architecture and provenance of the Xigaze forearc basin along the Yarlung Zangbo suture zone. Gondwana Research 22 (2), 415–433.
Wang, J., Hu, X.M., Garzanti, E., Wu, F.Y., 2013. Upper Oligocene–Lower Miocene Gangrinboche Conglomerate in the Xigaze area, southern Tibet: implications for Himalayan Uplift and Paleo-Yarlung-Zangbo Initiation. The Journal of Geology 121 (4), 425–444.
Wang, E., Kamp, P.J.J., Xu, G., Hodges, K.V., Meng, K., Lin, C., Luo, H., 2015. Flexural bending of southern Tibet in a retro foreland setting. Scientific Reports 5 (9). https://doi.org/10.1038/srep12076.
Wang, H.-Q., Ding, L., Cai, F.-L., Xu, Q., Li, S., Fu, J.-J., Lai, Q.-Z., Yue, Y.-H., Li, X., 2017. Early Tertiary deformation of the Zhongba–Gyangze Thrust in central southern Tibet. Gondwana Research 41, 235–248. https://doi.org/10.1016/j.gr.2015.02.017.
Wilke, F.D.H., Sobel, E.R., O'Brien, P.J., Stockli, D.F., 2012. Apatite fission track and (U–Th)/He ages from the Higher Himalayan Crystallines, Kaghan Valley, Pakistan: implications for an Eocene Plateau and Oligocene to Pliocene exhumation. Journal of Asian Earth Sciences 59, 14–23. https://doi.org/10.1016/j.jseaes.2012.06.014.
Wu, F.-Y., Ji, W.-Q., Wang, J.-G., Liu, C.-Z., Chung, S.-L., Clift, P.D., 2014. Zircon U–Pb and Hf isotopic constraints on the onset time of India-Asia collision. American Journal of Science 314 (2), 548–579.
Xu, Z., Dilek, Y., Yang, J., Liang, F., Liu, F., Ba, D., Cai, Z., Li, G., Dong, H., Ji, S., 2015. Crustal structure of the Indus–Tsangpo suture zone and its ophiolites in southern Tibet. Gondwana Research 27 (2), 507–524. https://doi.org/10.1016/j.gr.2014.08.001.
Yin, A., 2006. Cenozoic evolution of the Himalayan Orogen as constrained by alongstrike variations of structural geometry, exhumation history, and foreland sedimentation. Earth-Science Reviews 76, 1–134.
Yin, A., Harrison, T.M., 2000. Geologic evolution of the Himalayan–Tibetan orogen. Annual Review of Earth and Planetary Sciences 28, 211–280.
Yin, A., Harrison, T.M., Murphy, M., Grove, M., Nie, S., Ryerson, F., Le, C.Z., 1999. Tertiary deformation history of southeastern and southwestern Tibet during the Indo-Asian collision. Geological Society of America Bulletin 111 (11), 1644–1664.
Zeng, L., Gao, L.E., Xie, K., Liu-Zeng, J., 2011. Mid-Eocene high Sr/Y granites in the Northern Himalayan Gneiss Domes: melting thickened lower continental crust. Earth and Planetary Science Letters 303 (3), 251–266.
Zhang, Z.M., Zhao, G.C., Santosh, M., Wang, J.L., Dong, X., Shen, K., 2010. Late Cretaceous charnockite with adakitic affinities from the Gangdese batholith, southeastern Tibet: evidence for Neo-Tethyan mid-ocean ridge subduction? Gondwana Research 17, 615–631.

Zhu, D.C., Zhao, Z.D., Niu, Y.L., Mo, X.X., Chung, S.L., Hou, Z.Q., Wang, L.Q., Wu, F.Y., 2011. The Lhasa Terrane: record of a microcontinent and its histories of drift and growth. Earth and Planetary Science Letters 301 (1–2), 241–255.
Zhu, D.C., Zhao, Z.D., Niu, Y.L., Dilek, Y., Hou, Z.Q., Mo, X.X., 2013. The origin and pre-Cenozoic evolution of the Tibetan Plateau. Gondwana Research 23, 1429–1454.
Ziabrev, S., Aitchison, J., Abrajevitch, A., Davis, A., Luo, H., 2003. Precise radiolarian age constraints on the timing of ophiolite generation and sedimentation in the Dazhuqu terrane, Yarlung–Tsangpo suture zone, Tibet. Journal of the Geological Society of London 160 (4), 591–599. https://doi.org/10.1144/0016-764902-107.